# The Influence of Nanoparticles on Enzymatic Bioelectrocatalysis

*Dmitry Pankratov, Richard Sundberg, Dmitry B. Suyatin, Javier Sotres, Alejandro Barrantes, Tautgirdas Ruzgas, Ivan Maximov, Lars Montelius, and Sergey Shleev*

## Supporting Information

ABBREVIATIONS

3D, three-dimensional; $ABTS^{2-}$, 2,2'-azino-bis(3-ethylbenzthiazoline-6-sulphonic acid); $A_{geom}$, geometric surface area; $A_{real}$, real surface area; Au, gold; BSA, bovine serum albumin; CV, cyclic voltammogram; DET, direct electron transfer; $k_0$, standard heterogeneous electron transfer rate constants; $k_{cat}$, biocatalytic constant; $k_{cat}^{app}$, apparent bioelectrocatalytic constant; MCO, blue multi-copper oxidase; *Mv*BOx, *Myrothecium verrucaria* bilirubin oxidase; NHE, normal hydrogen electrode; NP, nanoparticle; $N_2$, molecular nitrogen; $O_2$, molecular oxygen; PBS, phosphate buffered saline; Si, silicon; $SiO_2$, silicon dioxide; *Th*Lc, *Trametes hirsuta* laccase; Ti, titanium.

**Section 1: Fabrication and characterisation of Au electrodes**

*Substrate preparation*. Square substrates with lateral size 8 × 8 $mm^2$, were prepared from 2", 250-300 μm thick *n*-type, <100> Si wafers from Siltronix (Archamps, France) using a Karl Süsscriber RA120 from SÜSS MicroTec AG (Garching, Germany). The $SiO_2$ layers of either 100, 300 or 500 nm thickness were thermally grown on the Si wafers through wet oxidation in Omega Junior diffusion furnace from Tempress A/S (Risskov, Denmark). The samples were cleaned with ultrasound agitation in isopropyl alcohol for 2 min and dried using a stream of $N_2$ gas.

*Thermal evaporation.* 5 nm thick film made of Ti (99.99+%) from Goodfellow (Cambridge, UK) and 100 nm thick film made of Au (99.9999%) from Dahlgren Ädelmetall (Malmö, Sweden) was deposited on the substrates in a custom-built thermal evaporator at a base pressure of $<10^{-6}$ mbar. Deposition rates were ~1 Å/s for Ti and ~10 Å/s for Au. The 5 nm thick layer of Ti was deposited to promote adhesion of the Au layer on the $SiO_2$ surface.

*Aerosol deposition.* Au particles with diameters of 20, 40, 60 and 80 nm (denoted $AuNPs_{20}$, $AuNPs_{40}$, $AuNPs_{60}$, $AuNPs_{80}$, respectively) were produced with an aerosol method in a custom built aerosol system[1] and deposited at a density of 70-100 particles per $\mu m^2$ (*ca.* 80 particles per $\mu m^2$) on the Au sample surface, which was prepared as described above.

*Electrode fabrication*. The fabricated samples with an Au surface were used as the working electrodes in the present study. For this, the samples were connected to a potentiostat using Au-plated alligator clips model 3289-2 from Pomona Electronics (Everett, WA, USA). A geometric area ( $A_{geom}$ ; also called two-dimensional projected area) of the electrodes was determined by direct precise geometric measurements using a vernier calliper from Mitutoyo Scandinavia AB (Upplands Väsby, Sweden).

*Electrode cleaning.* To clean the Au electrodes, as well as to make Au surfaces uniform on a molecular level, the electrodes were subjected to an oxidation-reduction cycle in 0.5 M $H_2SO_4$ between -0.1 and +1.9 V *vs.* normal hydrogen electrode (NHE) at a scan rate of 0.1 V $s^{-1}$ for just two cycles only, avoiding the agglomeration of AuNPs and their disappearance from the surface (Supporting Fig. S1). We recently demonstrated that the process underlying a simple method for the fabrication of 3D nanostructured Au electrodes from AuNPs is based on electrochemically driven transformation of physically deposited AuNPs into a genuinely 3D nanostructured material.[2] Thus, to avoid the formation of AuNP aggregates in the current studies, we used sub-monolayer coverage of surface with AuNPs, as well as limited electrochemical treatments of the electrodes to just two CV scans.

*Microscopy of Au electrodes.* Scanning electron microscopy (SEM) images of bare and AuNP-modified Au electrodes before and after electrochemical cleaning were made using FEI xtNova NanoLab 600 SEM infield immersion mode at 15 kV accelerating voltage and 2.2 nA beam current. Atomic force microscopy (AFM) images were obtained in water at room temperature (~25°C), by operating the AFM in the peak force tapping® (PFT) mode, *i.e.* when force curves are constantly performed at a constant rate equal to 2 kH, and the maximum load exerted on the sample is constantly and automatically minimised. When operating in the PFT® mode, triangular silicon nitride cantilevers with nominal spring constant 0.7 N $m^{-1}$, resonant frequency in air of 150 kHz and nominal tip radius of 20 nm were employed (*vide infra*). Analysis and processing of AFM images was performed with the WSxM software.[3] The standard image processing consisted of plane subtraction and/or equalisation. All samples (electrodes) were placed in the AFM liquid cell immediately after electrochemical cleaning and biomodification and were not allowed to dry at any moment to avoid possible enzyme deactivation.

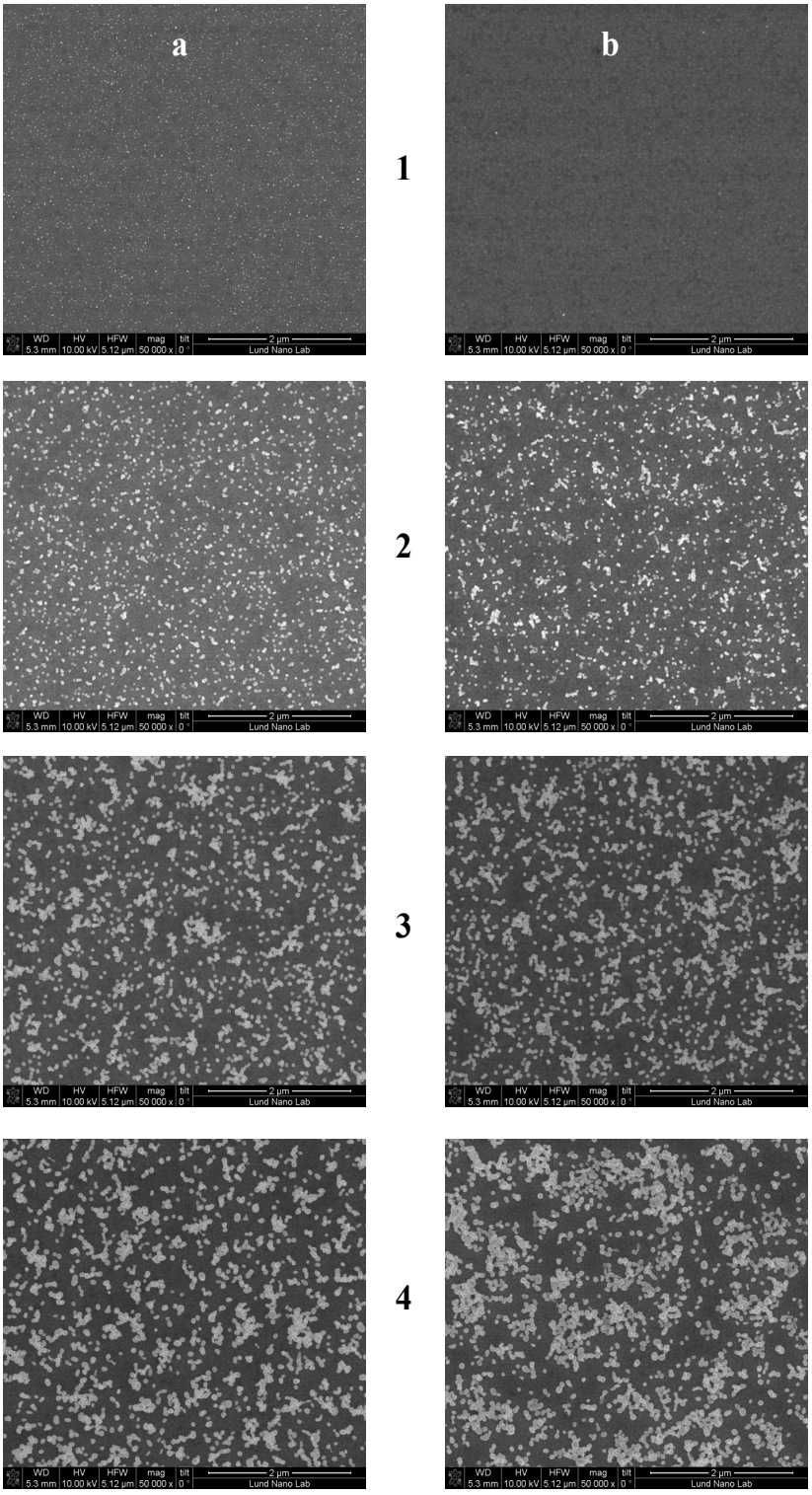


**Supporting Figure S1. SEM images of AuNP-modified electrodes** before (**a**) and after (**b**) 10 potentiodynamici cycles in 0.5 M $H_2SO_4$: 1 – $AuNPs_{20}$, 2 – $AuNPs_{40}$, 3 – $AuNPs_{60}$, 4 – $AuNPs_{80}$.

*Theoretical calculations of real surface area*. The real ( $A_{real}$ , also called microscopic or electrochemically active) electrode area of the Au electrodes was calculated taking into account $A_{geom}$ of the particular electrode, AuNPs size and their density on the electrode surface (Fig. 1a in the main text).

*Practical measurements of real surface area*. $A_{real}$ of Au electrodes was also calculated from the experimentally measured charge ( $q_{real}$ ) associated with the Au oxide reduction process performed by running CV from 0 to 1.9 V *vs.* NHE in 0.5 M $H_2SO_4$ (Supporting Eqn. S1). A current peak (Fig. 1c in the main text) related to the reduction of the gold was integrated to calculate $q_{real}$ . The theoretical charge density ( $\sigma_t$ ) associated with this process was taken to be 390 μC $cm_{real}^{-2}$.[4]

$$A_{real} = q_{real} / \sigma_t \quad \text{(S1)}$$

The microscopic roughness factors ( $f$ ) were calculated from Supporting Eqn. S2.

$$A_{real} = A_{geom} \times f \quad \text{(S2)}$$

**Section 2: Bio-modification of Au electrodes**

Clean Au electrodes with known $f$ values were biomodified by the simple adsorption of *Mv*BOx on the electrode surface using very dilute and very concentrated solutions of the enzyme (from 0.4 μg $mL^{-1}$ up to 4 mg $mL^{-1}$ in 10 mM phosphate buffer, pH 7.4) at room temperature (*ca.* 25°C). By taking into account the pI value of the enzyme, which is close to 4 (*vide infra*), one can conclude that the protein was negatively charged during immobilisation. It should be emphasised that the electrodes did not dry out at any time during modification and electrochemical investigations to avoid possible enzyme deactivation due to its dehydration.

**Section 3: Theoretical basis of bioelectrochemical investigations and modelling studies**

For proper mathematical elaboration of bioelectrochemical data, where a bioelectrocatalytic process has a mixed kinetics regime, possible diffusion limitations should be excluded, as presented below. In general, the rate of a bioelectrocatalytic process can be described by a mixed kinetics equation (Eqn. S3).

$$\frac{1}{i} = \frac{1}{i_{ET}} + \frac{1}{i_{cat}} + \frac{1}{i_{s-s}} \qquad \text{(S3)}$$

where, $i$ is the observed current, $i_{ET}$ is the limiting current of the heterogeneous electron transfer (ET; Supporting Eqn. S4; step 1 in Supporting Fig. S3 (*vide infra*), heterogeneous system, right panel), $i_{cat}$ is the limiting current of the biocatalytic process (Supporting Eqn. S5; step 3 in Supporting Fig. S3, heterogeneous system, right panel), and $i_{s-s}$ is the limiting diffusion current (Supporting Eqn. S6 at $\omega$ close to infinity).

$$i_{ET} = nFA_{real}k_0\Gamma \exp\left(\frac{-\alpha n' F(E - E^{0'})}{RT}\right) \qquad \text{(S4)}$$

$n'$ is the number of electrons in the slow electrochemical step, $F$ is the Faraday constant, $k_0$ is the standard heterogeneous ET constant, $\Gamma$ is the surface concentration of the enzyme, $\alpha$ is the charge transfer coefficient, $E$ is the electrode potential, $E^{0'}$ is the equilibrium potential of the electrode process, $R$ is the gas constant, and $T$ is the temperature in K.

If intramolecular ET (IET) is not a limiting step of the enzymatic process of $O_2$ bioelectroreduction (our previous studies of *Mv*BOx showed that this was the case at pH 7.4, ref.[5]), the bioelectrocatalytic current ($i_{cat}$) can be expressed as the electrochemical form of the Michaelis-Menten equation:

$$i_{cat} = \frac{nFA_{real}\Gamma k_{cat}^{app} C_{oxygen}}{C_{oxygen} + K_M} \quad \text{(S5)}$$

where $k_{cat}^{app}$ is the apparent rate constant for the bioelectrocatalytic process and $K_M$ is the Michaelis constant.

The Levich equation (Supporting Equation S6) defining steady-state current limited by the transport of substrate molecules at rotating electrode can be used to estimate mass-transfer limitations:

$$i_{s-s} = 0.62nFD^{2/3} C_{oxygen} A_{geom} \nu^{-1/6} \omega^{1/2} \quad \text{(S6)}$$

here, $i_{s-s}$ is the steady-state diffusion current, $n$ is the total number of electrons, $D$ is the diffusion coefficient of the substrate ($19.7 \cdot 10^{-6}$ cm$^2$ s$^{-1}$ for $O_2$), $C_{oxygen}$ is the bulk concentration of oxygen, $O_2$ ($2.5 \cdot 10^{-7}$mol cm$^{-3}$ and $1.2 \cdot 10^{-6}$ mol cm$^{-3}$ of $O_2$ (air and $O_2$ saturated solutions, respectively),[6] $\nu$ is the kinematic viscosity of the solution (0.01 cm$^2$ s$^{-1}$ at 25ºC, a typical value for aqueous solutions), and $\omega$ is the angular frequency (in rad s$^{-1}$).

To make a long story short, for the bioelectrocatalytic process strictly limited by $O_2$ diffusion, direct dependence between $C_{\text{oxygen}}$ and $j_{\text{max}}$ should be obtained, *i.e.* $j_{\text{max}}$ should have increased by a factor of 5, when the $O_2$ concentration was increased from 0.25 mM up to 1.2 mM. For electrocatalytic currents, which are limited by reaction kinetics, $j_{\text{max}}$ can be simply expressed as the electrochemical form of the Michaelis-Menten equation (Eqn. S5). When the $O_2$ concentration was increased from 0.25 mM up to 1.2 mM in our studies, *i.e.* when using $O_2$-saturated buffer instead of air-saturated 50 mM phosphate buffered saline (PBS, constituted of 50 mM $HPO_4^{2-}/H_2PO_4^-$ solution containing 0.15 M NaCl, pH 7.4), the maximal current density ($j_{\text{max}}$), which corresponds to bioelectrocatalytic $O_2$ reduction, increased by a factor of 2, *i.e.* from

12 $\mu$A $cm_{geom}^{-2}$ in air-saturated buffer to 25 $\mu$A $cm_{geom}^{-2}$ in $O_2$-saturated buffer, which follows Eqn. S5 suggesting just a minor $O_2$ diffusion limitation (*vide infra*).

In the present work, recorded CVs were analysed using the kinetic scheme recently elaborated by Climent *et al.*[7] If one does not take into account limitations due to $O_2$ mass transfer to the electrode surface, both $i_{ET}$ and $i_{cat}$ can be described based on the kinetic scheme presented below:

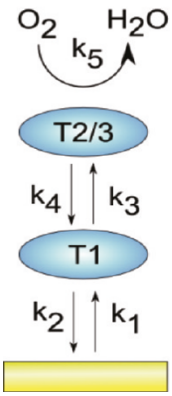


**Supporting Figure S2.** A kinetic scheme representing the bioelectrocatalytic mechanism of a blue multi-copper oxidase function (Supporting Fig. S3, heterogeneous catalysis, right panel, according to Ref.[7]).

The equations defining the currents are as follows:

$$i_{ET} = FA\Gamma[k_1(1-P_1) - k_2 P_1)] \quad \text{(S7)}$$

$$k_1 = k_0 \exp\left[-\alpha \frac{F}{RT}\left(E - E_{T_1}^{0'}\right)\right] \quad \text{(S8)}$$

$$k_2 = k_0 \exp\left[(1-\alpha)\frac{F}{RT}\left(E - E_{T_1}^{0'}\right)\right] \quad \text{(S9)}$$

$$k_5 = \frac{k_{cat}[O_2]}{K_M + [O_2]} \quad \text{(S10)}$$

where $k_1$ and $k_2$ are potential dependent DET rate constants defined by the Butler-Volmer formalism (Supporting Eqns S4, S8, and S9), whereas *P1* represents a fraction of adsorbed *Mv*BOx molecules with the reduced T1 copper centre (detail concerning *Mv*BOx structure are presented below).

The maximal bioelectrocatalytic current of $O_2$ electroreduction, as well as current dependence on the applied potential, can be described by the following summarised equation:

$$j = \frac{j_{\max}}{1 + \exp\left[\frac{F}{RT}\left(E - E_{T1}^{0'}\right)\right] + \frac{k_5}{k_0}\exp\left[\frac{\alpha F}{RT}\left(E - E_{T1}^{0'}\right)\right]} \qquad \text{(S11)}$$

Using this equation, modelling studies of obtained bioelectrocatalytic signals were performed (Fig. 3a) and basic parameters of bioelectrocatalytic reduction of $O_2$ were calculated (Supporting Table S1), by assuming $K_M$ and $\Gamma$ are equal to 0.2 mM and 3 pmol $cm_{real}^{-2}$, respectively.

**Supporting Table S1.** Basic bioelectrocatalytic parameters calculated using Supporting Equation S11 from modelling studies, *i.e.* using the kinetic scheme developed by Climent *et al.*

| Calculated parameters | without AuNPs | $AuNPs_{20}$ | $AuNPs_{40}$ | $AuNPs_{60}$ | $AuNPs_{80}$ |
|---|---|---|---|---|---|
| $k_0$ , $s^{-1}$ | 10.7 | 9.9 | 10.0 | 10.9 | 10.6 |
| $k_{cat}^{app}$ , $s^{-1}$ | 13.7 | 13.7 | 14.0 | 16.8 | 16.5 |
| $\alpha$ | 0.55 | 0.45 | 0.44 | 0.45 | 0.55 |

$\Gamma$ value equal to 3 pmol $cm_{real}^{-2}$ was obtained from ellipsometry studies (*vide infra*), whereas a $K_M$ value equal to 0.2 mM was taken from our previous investigations.[5] On the one hand, it is natural to use the $K_M$ value of the enzyme in homogeneous catalysis (*ca.* 0.2 mM) for heterogeneous systems, since the $K_M$ value towards $O_2$ for the adsorbed *Mv*BOx coincides with the values obtained in homogeneous reactions.[5] On the other hand, it is well-known that apparent $K_M$ values of the adsorbed *Mv*BOx towards $O_2$ greatly depend on the potential applied. Thus, it is important to emphasise that neither $k_0$ nor $k_{cat}^{app}$ dependences on AuNP sizes presented in Fig. 3c (main text) will be even slightly modified, if different $K_M$ or $\Gamma$ values are used for calculations, *e.g.* if another $K_M$ value is assumed following the region of constants reported in

the literature, 0.1 mM – 1 mM.[5, 8]. In other words, variation of these parameters, *viz.* both $K_M$ and $\Gamma$ values, during the modelling, will not change the main conclusion made in our studies.

**Section 4: AFM studies**

The Au grains were completely covered by globular features with average lateral dimensions of *ca.* 20 nm, when concentrated enzyme solution (4 mg $mL^{-1}$) was used for biomodification (Fig. 2d in the main text). While this width is longer than that expected for a single *Mv*BOx molecule (*ca.* 5 nm; details concerning enzyme structure are in section 6 of SI, Supporting Fig. S3), it is well-known that visualisation of features smaller than the AFM tip results in width values similar to those of the tip (*ca.* 20 nm) due to tip dilation effects;[9] this is probably the case in our experiments. Thus, it is likely that the topography images show the convolution of the AFM tip and the molecules protruding from the surface. Nevertheless, it is reasonable to assume *i*) from the homogeneity of the samples and *ii*) from the fact that the images do not show zones of the substrate without molecules, that full coverage was obtained. *Mv*BOx was also adsorbed on bare Au electrodes using a dilute enzyme solution (0.25 mg $mL^{-1}$) in order to obtain sub-monolayer coverage. These *Mv*BOx/Au samples showed isolated globular features on top of the wider Au grains (Fig. 2c in the main text), which exhibited lateral and vertical dimensions of *ca.* 20 nm and 3.0±0.8 nm, respectively. As in the case of fully covered samples, the molecules exhibiting larger lateral dimensions than those expected for single molecules can be attributed to tip dilation effects.[9] The *Mv*BOx molecules exhibiting a lower height than that expected (*ca.* 5 nm; *vide infra*) can be attributed to tip compression effects.[10] It is important to emphasise that no desorption of *Mv*BOx from the electrode surface was registered by AFM when modified

electrodes were kept in buffer solution for 1 h, indicating that the adsorption of the enzyme on Au has an irreversible character. These results are in very good agreement with our recently published data concerning interfacial behaviour and the activity of *Mv*BOx on bare polycrystalline gold surface.[11]

**Section 5: Ellipsometry studies**

The adsorption of *Mv*BOx onto bare Au was studied *in situ* by means of null ellipsometry, which measures changes in the polarisation of light reflected by a surface. The Au surface was vertically mounted in a glass trapezoid cuvette (Hellma, Germany) containing 4 mL of solution, which was thermostated at 25°C and stirred using a magnetic stirrer with a rotation speed of 325 rpm. The changes in ellipsometric angles were recorded *in situ* every 15 sec. In order to determine the refractive index of the Au surface, a four-zone surface calibration in buffer solution was carried out prior to each measurement. When enzymes were to be adsorbed on the electrochemically cleaned Au surface, first, a stable baseline acquisition was done, and then a dilute solution of *Mv*BOx (0.25 mg $mL^{-1}$) was added to the cuvette to a final volume of 4 mL. The formation of protein films was monitored for 60 min, followed by rinsing with enzyme-free buffer solution for 5 min. From ellipsometric data, the adsorbed amount per unit area ( $\Gamma$ , in mg $m^{-2}$ using measured $A_{geom}$ ) was calculated assuming a 3 layer model (Au-Enzyme layer-Buffer solution) and using a value of 0.18 mL $g^{-1}$, as the refractive index increment with respect to change in protein concentration ( $dn / dc$ ).[12] $\Gamma$ value of 2.8 ± 0.1 mg $m^{-2}$ was obtained, *i.e.* 4.8 pmol $cm_{geom}^{-2}$ taking into account the molecular weight of *Mv*BOx equal to 59 kDa (*vide infra*). When the value was recalculated to $A_{real}$, taking into account *f* of bare planar Au electrodes equal to 1.8, 2.7 pmol $cm_{real}^{-2}$ (*ca.* 3 pmol $cm_{real}^{-2}$) was obtained and used in all calculations of catalytic

constants (*vide supra*). It is important to emphasise that no desorption of *Mv*BOx from the electrode surface was registered by ellipsometry measurements when rinsing with enzyme-free buffer solution after modification, additionally confirming that the adsorption of the enzyme on Au has irreversible character in the experimentally relevant time frame. These results are in very good agreement with our recently published data concerning interfacial behaviour and activity of MvBOx on bare polycrystalline gold surface.[11]

**Section 6: Mechanism of MCO functions**

Nowadays, mechanisms of MCO functions during homogeneous and heterogeneous reactions are quite well-understood and include three major steps:

1 – ET from an enzyme substrate (in homogeneous or heterogeneous systems, *i.e.* when an enzyme is in solution or in an adsorbed state) or an electrode (heterogeneous system, *i.e.* when enzyme is adsorbed on the electrode; Supporting Fig. S3, right) to a mononuclear Cu-T1 site.

2 – intramolecular ET (IET) from the Cu-T1 site to a Cu-T23 cluster *via* a highly conserved Cys–2His ET pathway across a distance of *ca.* 13 Å.

3 – $O_2$ reduction to two $H_2O$ molecules by the trinuclear Cu cluster (Cu-T23; Supporting Fig. S3).[13-15]

*Myrothecium verrucaria* bilirubin oxidase (*Mv*BOx) preparation (Amano 3) was received from Amano Enzyme Inc. (Nagoya, Japan) as a kind gift from the company. The preparation was additionally purified at the Bach Institute of Biochemistry (Moscow, Russia). The *Mv*BOx solution used in the present studies is thus a highly purified preparation of the enzyme (to avoid possible artefacts related to impurities in enzyme preparation) with only one minor band in SDS-

PAGE of a lower molecular mass, which, based on previous studies,[8] can be attributed to some degradation products of the enzyme (Supporting Fig. S4).

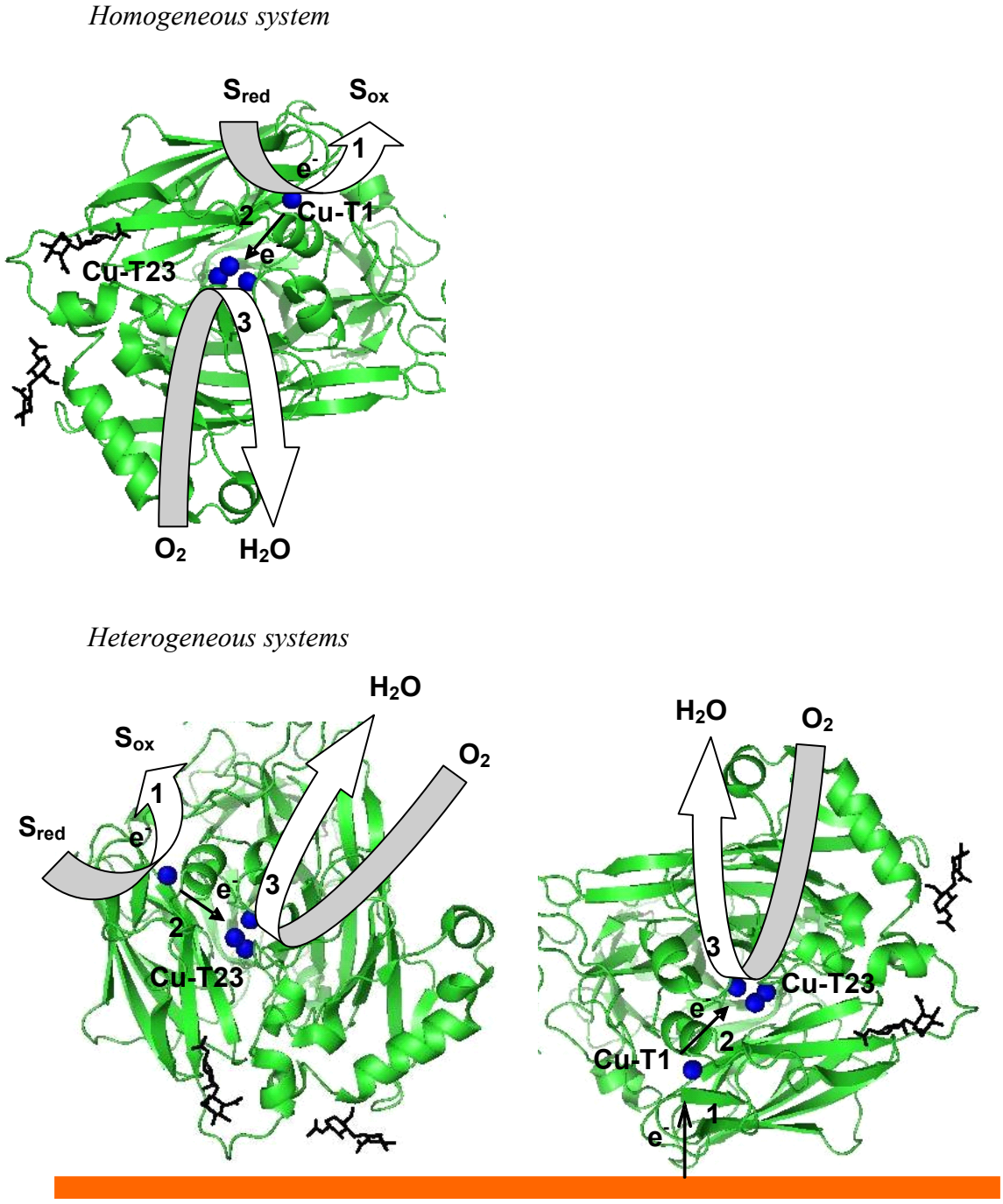


**Supporting Figure S3.** Crystal structure of (PDB 2XLL) and schematic representation of two mechanisms of MCO functions during homogeneous and heterogeneous reactions. Protein globule – green ribbons; copper ions – blue spheres, and carbohydrates – black sticks.

**Section 7: Redox enzyme**

MCO is a glycated protein with a molecular weight of ~59 kDa. The approximate molecular weight for *Mv*BOx is given since many significantly different values can be found in the literature for this enzyme, ranging *e.g.* from 52.0 kDa in ref.[16] up to 64.2 kDa in ref.[8] However, according to SDS-PAGE (Supporting Fig. S4), the *Mv*BOx used in our studies has a molecular weight of about 59 kDa, which is a good average value taking into account reports existing in the literature. The crystal structure of the redox enzyme is presented in Supporting Fig. S3. Based on the structure, one can estimate the size of *Mv*BOxto be 40×50×60 Å.[17] The pI value of *Mv*BOx was previously found to be 4.1.[16]

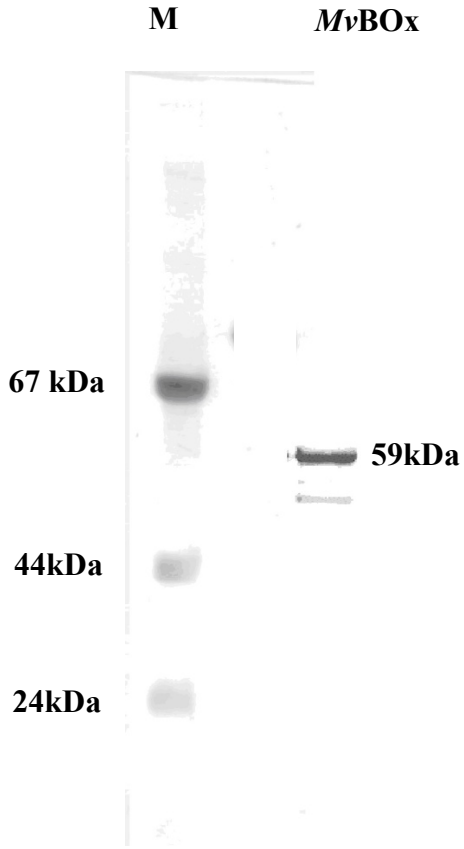


**Supporting Figure S4.** SDS-PAGE of *Mv*BOx preparation used in the present studies (M - molecular mass rulers).

The specific activity of *Mv*BOx in homogeneous solution was determined by estimation of the initial rates of $O_2$ consumption using an Oxygraph Clark $O_2$ electrode with constant stirring at room temperature (25°C). The general reaction mechanism is presented in Fig. 3d in the main text of the manuscript. *Mv*BOx is able to efficiently oxidize 2'-azino-bis(3-ethylbenzthiazoline-6-sulphonic acid) ($ABTS^{2-}$) with concomitant reduction of $O_2$ to $H_2O$.[18, 19] An appropriate $ABTS^{2-}$ dissolved in PBS was used in order to ensure a measurable linear rate for the first 30 s after the addition of enzyme preparation. The concentration of $O_2$ was assumed to be 0.25 mM and 1.2 mM in air- and $O_2$-saturated buffers, respectively.[6] The biocatalytic constant ($k_{cat}$) for *Mv*BOx in homogeneous reaction was calculated by taking into account enzyme concentration determined spectrophotometrically using bovine serum albumin (BSA) as a standard.[20] The calculated biocatalytic constant ($k_{cat}$) of *Mv*BOx towards ABTS in 50 mM PBS was found to be 57 $s^{-1}$ at 25ºC.

**Section 8: Chemicals and equipment**

$Na_2HPO_4{\cdot}2H_2O$, $NaH_2PO_4{\cdot}H_2O$, NaCl, and $H_2SO_4$ were obtained from Sigma-Aldrich (St. Louis, MO, USA). Isopropyl alcohol was purchased from Merck (Darmstadt, Germany). All chemicals were of analytical grade and used without further purification. Molecular $O_2$ was obtained from AGA Gas AB (Sundbyberg, Sweden). Buffers and all other solutions were prepared using deionised water (18 MΩcm) purified with a PURELAB UHQ II system from ELGA Labwater (High Wycombe, UK). The measurements were performed at room temperature (25ºC) using PBS.

Electrochemical measurements were carried out using a μAutolab Type III/FRA2 potentiostat/galvanostat from Metrohm Autolab B.V. (Utrecht, The Netherlands). While using a

three-electrode configuration, an $Hg|Hg_2Cl_2|KCl_{sat}$ (SCE, 242 mV *vs.* NHE) and a platinum wire mesh were applied as reference and counter electrodes, respectively. Ultrasonication was performed using an Ultrasonic Cleaner XB2 from VWR International Ltd. (East Grinstead, West Sussex, UK).

Scanning electron microscopy (SEM) was performed using an ultra-high resolution scanning electron microscope FEI Nova NanoLab 600 from FEI (Eindhoven, Netherlands).

Atomic force microscopy (AFM) images of Au surfaces were obtained using a liquid cell MultiMode 8 SPM with a NanoScope V control unit from Bruker AXS (Karlsruhe, Germany). Commercially available tips Scan Asyst-Fluid from Bruker AXS were employed.

A thin film automated ellipsometer (type 43 603-200E, Rudolph Research, Fairfield, NJ, USA) equipped with a xenon arc lamp with a fixed angle of incidence (67.96°) was used in ellipsometry studies. Light was detected at a wavelength of 442.9 nm employing an interference filter with ultraviolet and infrared blocking (MellesGriot, Netherlands).

An Oxygraph Clark $O_2$ electrode from Hansatech Ltd. (Norfolk, England) was used for determination of the specific activity of *Mv*BOx.

**Supporting References:**


1. M. H. Magnusson, K. Deppert, J.-O. Malm, J.-O. Bovin and L. Samuelson, *J. Nanopart. Res.*, 1999, 1, 243-251.
2. V. Andoralov, M. Falk, B. Suyatin Dmitry, M. Granmo, J. Sotres, R. Ludwig, O. Popov Vladimir, J. Schouenborg, Z. Blum and S. Shleev, *Scientific reports*, 2013, 3, 3270.
3. I. Horcas, R. Fernandez, J. M. Gomez-Rodriguez, J. Colchero, J. Gomez-Herrero and A. M. Baro, *Rev. Sci. Instrum.*, 2007, 78, 013705/013701-013705/013708.
4. S. Trasatti and O. A. Petrii, *Pure Appl. Chem.*, 1991, 63, 711-734.
5. S. Shleev, V. Andoralov, M. Falk, C. T. Reimann, T. Ruzgas, M. Srnec, U. Ryde and L. Rulisek, *Electroanalysis*, 2012, 24, 1524-1540.
6. G. A. Truesdale and A. L. Downing, *Nature*, 1954, 173, 1236.

7. V. Climent, J. Zhang, E. P. Friis, L. H. Oestergaard and J. Ulstrup, *J. Phys. Chem. C*, 2012, 116, 1232-1243.
8. L. dos Santos, V. Climent, C. F. Blanford and F. A. Armstrong, *Phys. Chem. Chem. Phys.*, 2010, 12, 13962-13974.
9. E. Margeat, C. Le Grimellec and C. A. Royer, *Biophys. J.*, 1998, 75, 2712-2720.
10. F. Moreno-Herrero, J. Colchero and A. M. Baro, *Ultramicroscopy*, 2003, 96, 167-174.
11. D. Pankratov, J. Sotres, A. Barrantes, T. Arnebrant and S. Shleev, *Langmuir*, 2013.
12. J. A. De Feijter, J. Benjamins and F. A. Veer, *Biopolymers*, 1978, 17, 1759-1772.
13. S. Tsujimura, T. Nakagawa, K. Kano and T. Ikeda, *Electrochemistry (Tokyo)*, 2004, 72, 437-439.
14. S. Shleev, A. Jarosz-Wilkolazka, A. Khalunina, O. Morozova, A. Yaropolov, T. Ruzgas and L. Gorton, *Bioelectrochemistry*, 2005, 67, 115-124.
15. T. Sakurai and K. Kataoka, *Chem. Rec.*, 2007, 7, 220-229.
16. N. Tanaka and S. Murao, *Agricultural Biol. Chem.*, 1982, 46, 2499-2503.
17. J. A. Cracknell, T. P. McNamara, E. D. Lowe and C. F. Blanford, *Dalton Trans.*, 2011, 40, 6668-6675.
18. A. Trifonov, K. Herkendell, R. Tel-Vered, O. Yehezkeli, M. Woerner and I. Willner, *ACS Nano*, 2013, 7, 11358-11368.
19. S. Tsujimura, H. Tatsumi, J. Ogawa, S. Shimizu, K. Kano and T. Ikeda, *J. Electroanal. Chem.*, 2001, 496, 69-75.
20. B. Ehresmann, P. Imbault and J. H. Weil, *Anal. Biochem.*, 1973, 54, 454-463.